Radiation and Conduction Heat Transfer Coupled with Liquid Water Transfer, Moisture Sorption, and Condensation in Porous Polymer Materials

Z. Wang, Y. Li, Q. Y. Zhu, Z. X. Luo

Institute of Textiles and Clothing, the Hong Kong Polytechnic University, Hung Hom, Kowloon, Hong Kong

Received 21 June 2002; accepted 5 November 2002

ABSTRACT: A new one-dimensional mathematical model to simulate the complex coupled heat and moisture transfer in porous polymer materials is presented. The new model takes into account effects of multiple involved processes such as radiation and conduction heat transfer, liquid capillary action, moisture sorption, and condensation. The technique of volume of fraction (VOF) is used to model the dynamic distribution of moisture in different phases, that is, vapor and liquid. The finite volume method (FVM) is used to develop the numerical computational scheme to solve the model. The temperature change on the fabric surface derived from the computational results of the model is compared with experimental measurements with reasonable agreement between the two. Further numerical simulations were carried out to investigate the complex interactions and coupling effects among the various heat and moisture-transfer processes involved. © 2003 Wiley Periodicals, Inc. J Appl Polym Sci 89: 2780–2790, 2003

Key words: diffusion; modeling; fibers; coupled heat and moisture transfer; porous material

INTRODUCTION

As the pioneer, Henry[1] reported a relatively simple mathematical model to describe coupled heat and moisture transfer in a bale of cotton fibers, which was further developed and improved to take into account various complex and interrelated physical mechanisms. The heat transfer involves conduction by the solid material of the fibers and intervening air,[2] by radiation attributed to the large temperature difference, and by convection when air penetrates the porous material.[3] Meanwhile, moisture transfer involves vapor diffusion in the void space, moisture diffusion in fibers (i.e., sorption/adsorption),[4–6] condensation/evaporation at fiber surface, and liquid transfer inside the fabric by capillary effects.[7–9] Because of the heat released or absorbed during the processes of phase change, such as sorption/adsorption and condensation/evaporation, the heat transfer is coupled with the moisture transfer processes.[10,11] In addition, the transport of the liquid across the porous material increases the medium's thermal conductivity and changes the behavior of heat transfer as well as the moisture absorption of fibers.

Correspondence to: Y. Li (tcliyi@polyu.edu.hk).

Contract grant sponsor: Hong Kong Research Grant Committee; contract grant number: PolyU5111/98E.

Contract grant sponsor: Hong Kong Polytechnic University.

Journal of Applied Polymer Science, Vol. 89, 2780–2790 (2003)

Gibson developed a series governing equations that describe the transient heat and mass transfer through hygroscopic porous media using volume-averaging techniques.[12] The model was applied to study the interactions between the human thermoregulation and the clothing layers.[13] He also applied the simplified 1-D form of those equations to predict the behavior of transient diffusion of couple heat and moisture flow through groups of porous polymer materials made of different textile fibers[14] and obtained good agreement with the experimental temperature profiles of the materials. At the end of the study,[14] Gibson also discussed taking the effect of thermal radiation into account at the boundary heat transfer and provided a simple form for the effective heat transfer coefficient by combining the convective and thermal radiative transfer coefficient in a linear way.

Farnworth pointed out that under circumstances of large temperature differences, radiative heat flow is about the same as the conductive heat flow, and thus should not be ignored. By incorporating the thermal radiation model through the clothing insulation developed by Farnworth,[3] Luo et al. improved the original mathematical model for the coupled heat and moisture transfer through the hygroscopic textile fabrics[15] to the porous clothing assembly with consideration of the moisture sorption mechanisms and the condensation process.[16] However, the condensation term in their model cannot describe the physical mechanism of condensation/evaporation process and be distinguished from the sorption/adsorption process. Moreover, the whole model does not take into account the

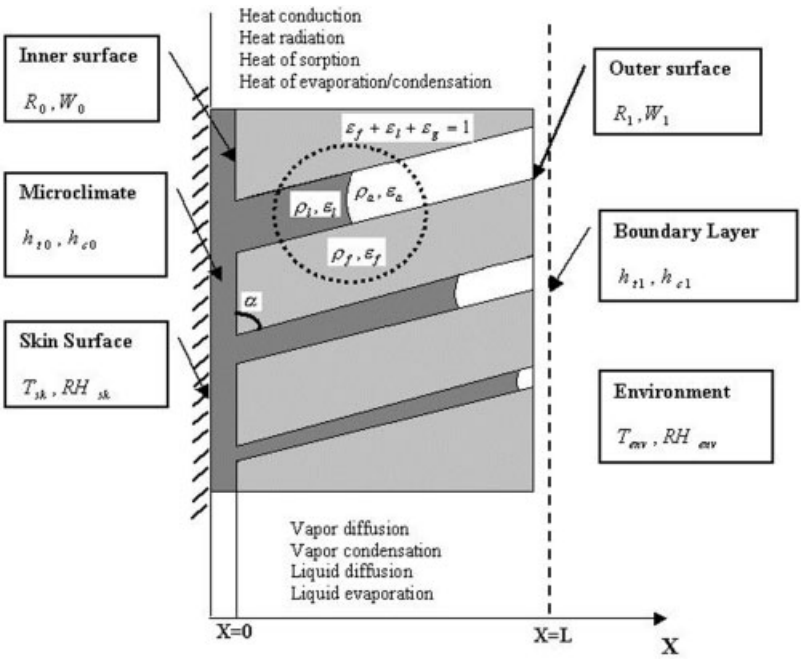

Figure 1 Schematic diagram of the model.

liquid capillary transport processes. To overcome these problems, Li et al.[11] developed a new model by using the technique of volume of fraction (VOF). In their model, the mechanism of capillary action was considered, and was incorporated into the mass conservation equation for the liquid volumetric fraction. The new model is able to illustrate the dynamic distribution of liquid water, water vapor in void space in the fabric, and the water content in hygroscopic fibers.

In this study, we report a new mathematical model that incorporates the complex physical mechanisms of the radiative and conductive heat transfer processes coupled with capillary action, moisture diffusion through the porous polymer materials, and the inside phase change processes such as moisture condensation/evaporation and moisture sorption/adsorption by the fibers. We also developed a numerical solution scheme for the model and compare the simulated temperature profile of the fabric sample surface with experimental measurements. Further, we report two cases of numerical simulation, in which a porous polymer slab is exposed to large temperature and moisture gradients at the two sides with and without direct contact of liquid on the inner surface to illustrate and compare the complex mechanisms involved in the cases.

MECHANISMS AND MATHEMATICAL FORMULATION

Description and assumptions of the model

Figure 1 shows a piece of porous polymer slab as part of clothing assembly with two thin fabrics/films attached at the two surfaces. The inner side is close to the human skin and the outer surface is interfaced to the external environment. The internal structure of the porous polymer materials is assumed to be composed of capillaries that are made up of interconnected pores formed by polymer fibers. The distribution of liquid, water vapor in any tiny element inside the slab is described by a relationship of volumetric fractions $\varepsilon_l + \varepsilon_a = 1 - \varepsilon_f$. Liquid water can then be propelled by capillary action from regions of higher liquid content to the drier regions. $x = 0$ and $x = L$ denote the positions at the inner and outer surfaces of the porous slab, respectively.

In developing the model, we made the following assumptions:

1. The porous polymer slab is isotropic in terms of structure and thermal properties.
2. Local thermal equilibrium exists among all phases because of the relatively low velocities considered and the small dimensions of the constituting fibers.
3. The angular distribution of radiative intensity is approximately constant, and the scattering of radiation by the fibers can be ignored.
4. Instant equilibrium is reached between the moisture content at fiber surface and that of the surrounding air.
5. The air–vapor mixture reaches saturation instantly in the presence of liquid.
6. Swelling of the fibers attributed to absorbing moisture can be neglected.
7. The inertial force is ignored because of the relatively low velocities for liquid transfer.

Governing equations

The following mathematical governing equations are established on the basis of the above assumptions. Equations (1) and (2) show the mass conservation of moisture vapor and liquid, respectively, and eq. (3) describes the energy conservation.

$$\frac{\partial(C_a\varepsilon_a)}{\partial t} = \frac{1}{\tau_a}\frac{\partial}{\partial x}\left(D_a\frac{\partial(C_a\varepsilon_a)}{\partial x}\right) - \bar{\omega}_1\Gamma_f + \Gamma_{lg} \quad (1)$$

$$\frac{\partial(\rho_l\varepsilon_l)}{\partial t} = \frac{1}{\tau_l}\frac{\partial}{\partial x}\left(D_l(\varepsilon_l)\frac{\partial(\rho_l\varepsilon_l)}{\partial x}\right) - \bar{\omega}_2\Gamma_f - \Gamma_{lg} \quad (2)$$

$$c_\nu\frac{\partial T}{\partial t} = \frac{\partial}{\partial x}\left(K_{mix}(x)\frac{\partial T}{\partial x}\right) + \frac{\partial F_R}{\partial x} - \frac{\partial F_L}{\partial x} + \bar{\omega}_1\lambda_\nu\Gamma_f + \bar{\omega}_2\lambda_l\Gamma_f - \lambda_{lg}\Gamma_{lg} \quad (3)$$

The mathematical descriptions for the processes of liquid transfer, moisture sorption/desorption, and condensation/evaporation, as well as the radiative heat transfer are explained in following text. Exact definitions for the symbols can be found in the Nomenclature section.

The liquid diffusivity $D_l(\varepsilon_l)$ in eq. (2) is derived from the physical mechanisms of capillary theory and Darcy's law for the liquid transfer through the porous media and is expressed as[11]

$$D_l(\varepsilon_l) = \frac{\gamma\cos\varphi\sin^2\alpha d_c\varepsilon_l^{1/3}}{20\eta\varepsilon^{1/3}} \quad (4)$$

Equation (5) indicates the evaporation/condensation rate of the liquid/moisture, where the volumetric fraction of vapor ε_a denotes the void space for liquid water evaporation and the moisture vapor condensation.

$$\Gamma_{lg} = \varepsilon_a h_{lg} S_\nu(C^*(T) - C_a) \quad (5)$$

Equation (6) describes the moisture sorption of the fibers according to the second Fick's law for a cylinder coordinate system. The moisture vapor diffusion coefficient D_f related by the water content inside the fiber $W_{cf}(x, t)$, and the moisture content at the fiber surface are determined by the relative humidity (RH) of the surrounding air at the time–space position of (x, t), as shown in eq. (7).

$$\Gamma_f = \frac{\partial(C_f\varepsilon_f)}{\partial t} = \frac{1}{r}\frac{\partial}{\partial r}\left(rD_f\frac{(C_f\varepsilon_f)}{\partial r}\right) \quad (6)$$

$$C_{fs}(x, R_f, t) = f(RH_a(x, t), T(x, t)) \quad (7)$$

The proportions of moisture sorption at the fiber surfaces covered by liquid and/or covered by air at any position (x, t) are described by two factors ω_1 and ω_2, whose relationship is determined by eq. (8).

$$\bar{\omega}_1 + \bar{\omega}_2 = \frac{\varepsilon_a}{\varepsilon} + \frac{\varepsilon_l}{\varepsilon} = 1 \quad (8)$$

Equations (9) and (10) give the attenuation of the thermal radiation fluxes, but ignore the scattering of radiation by fibers inside the slab. The total thermal radiation incident on a tiny volume element inside the slab traveling to the right and left direction is denoted, respectively, by F_R and F_L; the fraction of F_R or F_L that is absorbed by the fibers in a volume element is characterized by the absorption constant β.[3]

$$\frac{\partial F_R}{\partial x} = -\beta F_R + \beta\sigma T^4 \quad (9)$$

$$\frac{\partial F_L}{\partial x} = \beta F_L - \beta\sigma T^4 \quad (10)$$

$$\beta = \frac{(1-\varepsilon)}{r}\varepsilon_r \quad (11)$$

K_{mix} is the effective thermal conductivity for the porous polymer slab, and is defined as eq. (12),[16] where K is the dynamic thermal conductivity of the wetted slab, and can be obtained from experiments[2] or empirical equations[17]; K_l is the thermal conductivity of the liquid water.

$$K_{mix} = \varepsilon_l K_l + (\varepsilon_l + \varepsilon_f)K \quad (12)$$

Initial and boundary conditions

We assumed that a porous polymer slab is initially equilibrated to a given skin surface and atmospheric condition in terms of temperature and the vapor concentration (T_{sk0}, C_{sk0}) and (T_{env0}, C_{env0}) with linear distributions across the thickness of the slab.

At the position $x = 0$, different boundary conditions are specified for the situations of direct and nondirect contact with liquid water as follows:

No direct contact with liquid water

$$\left.\begin{aligned} &D_a\frac{\partial(C_a\varepsilon_a)}{\partial x}\Big|_{x=0} = H_{c0}(C_a - C_{sk}) \\ &\varepsilon_l(0, t) = 0 \\ &K_{mix}\frac{\partial T}{\partial x}\Big|_{x=0} = H_{t0}(T - T_{sk}) \\ &F_R(0, t) = (1-\varepsilon_0)F_L(0, t) + \varepsilon_0\sigma T^4(0, t) \end{aligned}\right\} \quad (13a)$$

Direct contact with liquid water

$$\left.\begin{aligned} &C_a(0,\,t) = C^*(T)\\ &\varepsilon_l(0,\,t) = 1 - \varepsilon_f\\ &K_{mix}\left.\frac{\partial T}{\partial x}\right|_{x=0} = H_{t0}(T - T_{sk})\\ &F_R(0,\,t) = (1-\varepsilon_0)F_L(0,\,t) + \varepsilon_0\sigma T^4(0,\,t) \end{aligned}\right\} \quad (13b)$$

At $x = L$, the boundary conditions are described by the following equations with consideration of the convective nature of the boundary air layers:

$$\left.\begin{aligned} &D_a\left.\frac{\partial(C_a\varepsilon_a)}{\partial x}\right|_{x=L} = -\kappa_1 H_{c1}(C_a - C_{env})\\ &K_{mix}\left.\frac{\partial T}{\partial x}\right|_{x=L} = -H_{t1}(T - T_{env}) - \kappa_2\lambda_{lg}h_{lg}(C^*(T) - C_{env})\\ &D_l\rho_l\left.\frac{\partial \varepsilon_l}{\partial x}\right|_{x=L} = -\kappa_2 h_{l\to g}(C^*(T) - C_{ab})\\ &F_L(L,\,t) = (1-\varepsilon_1)F_R(L,\,t) + \varepsilon_1\sigma T^4(L,\,t) \end{aligned}\right\} \quad (14)$$

The proportions of the mass transfer at $x = L$ by vapor transport and that by the liquid water are denoted by $\kappa_1 = \varepsilon_a/\varepsilon$ and $\kappa_2 = \varepsilon_l/\varepsilon$, respectively. In eqs. (13) and (14), H_c and H_t are the combined mass transfer and the combined heat transfer coefficients denoting the various thermal and moisture-transfer resistance expressed as:

$$H_{cn} = \frac{1}{W_n + \dfrac{1}{h_{cn}}} \quad (14a)$$

$$H_{tn} = \frac{1}{R_n + \dfrac{1}{h_{tn}}} \quad (14b)$$

where $n = (0, 1)$ for the inner and outer surface of the slab, respectively; W_n and R_n are the resistance of the moisture vapor and heat transfer of the surfaces of the slab, respectively; and h_{cn} and h_{tn} are the mass and heat transfer coefficients, respectively.

NUMERICAL SCHEME FOR THE MODEL

The finite volume method is used to construct the numerical scheme on the basis of work reported in Li et al.[11] and Luo et al.[16] Along the direction of thickness L, the slab is divided into $(n + 1)$ control cells with equal interval size. Each control cell is regarded as being composed of different volumetric fractions of liquid water ε_l and void space ε_a.

Let $\omega = \Delta x^2/\Delta t$, $\mu_g = D_g/\tau_g$, $\mu_l = D_l(\varepsilon_l)/\tau_l$, $\mu_f = \Delta t D_f/\Delta r^2$, and $\Phi = \lambda_f\omega_1\Gamma_f + \lambda_l\omega_2\Gamma_f - \lambda_{lg}\Gamma_{lg}$. The final discrete equations are generated with a fully implicit scheme as follows:

$$\frac{\mu_a}{\omega}(C_a\varepsilon_a)_{j+1}^{n+1} - \left(2\frac{\mu_a}{\omega} + 1\right)(C_a\varepsilon_a)_j^{n+1} + \frac{\mu_a}{\omega}(C_a\varepsilon_a)_{j-1}^{n+1} = (C_a\varepsilon_a)_j^n + \Delta t(\varepsilon_a)_j^n h_{l\to g}S_v(C^*(T_j^n) - (C_a)_j^n) - \bar{\omega}_1\Delta t(\Gamma_f)_j^n \quad (15)$$

$$\frac{\mu_l}{\rho_l\omega}(\varepsilon_l)_{j-1}^{n+1} - \left(2\frac{\mu_l}{\rho_l\omega} + 1\right)(\varepsilon_l)_j^{n+1} + \frac{\mu_l}{\rho_l\omega}(\varepsilon_l)_{j-1}^{n+1} = (\varepsilon_l)_j^n - \Delta t\frac{\mu_l}{\rho_l\omega}(\varepsilon_a)_j^n h_{gl}S_v(C^*(T_j^n) - (C_a)_j^n) - \bar{\omega}_2\Delta t(\Gamma_f)_j^n \quad (16)$$

$$\left.\begin{aligned} &A_j^{n+1}T_{j-2}^{n+1} + B_j^{n+1}T_{j-1}^{n+1} + C_j^{n+1}T_j^{n+1} + D_j^{n+1}T_{j+1}^{n+1} + E_j^{n+1}T_{j+2}^{n+1} = F_j^{n+1}\\ &A_j^{n+1} = KK_{j-2}\\ &B_j^{n+1} = -((3 + \Delta x^2\beta^2)KK_{j-1} + KK_{j-2} + \omega(c_\nu)_{j-1} - 8\beta\sigma(T_j^n)^3\Delta x^2)\\ &C_j^{n+1} = (3 + \Delta x^2\beta^2)(KK_j + KK_{j-1}) - 16\beta\sigma(T_j^n)^3\Delta x^2 + \omega(c_\nu)_j(2 + \Delta x^2\beta^2)\\ &D_j^{n+1} = -((3 + \Delta x^2\beta^2)KK_j + KK_{j+1} + \omega(c_\nu)_{j+1} - 8\beta\sigma(T_j^n)^3\Delta x^2)\\ &E_j^{n+1} = KK_{j+1}\\ &F_j^{n+1} = -\omega((c_\nu)_{j+1}T_{j+1}^n + 2(c_\nu)_j T_j^n - (c_\nu)_{j-1}T_{j-1}^n) - 24\beta\sigma\Delta x^2(T_j^n)^2\\ &\qquad \times (T_{j+1}^n - T_j^n)^2 + \beta^2(c_\nu)_j\Delta x^2\omega T_j^n - \Delta x^4\left(\left(\frac{\partial^2\Phi}{\partial x^2}\right)_j^n - \beta^2\Phi_j^n\right) \end{aligned}\right\} \quad (17)$$

where

$$(\Gamma_f)_j^n = \frac{\varepsilon_f}{\Delta t}\chi\left(\sum_{k=1:R_f}(\mu_f)_k^n\left(\left(1 + \frac{1}{2k}\right)(C_f)_{k+1}^n - 2(C_f)_k^n + \left(1 - \frac{1}{2k}\right)(C_f)_{k-1}^n\right)\right)_j^n \quad (18)$$

$$KK_j = \frac{1}{2}(K_j + K_{j+1}) \quad (19)$$

$\chi(\bullet)_j^n$ is an averaging operator in the cell j.

The calculation flow of the model is described in Figure 2.

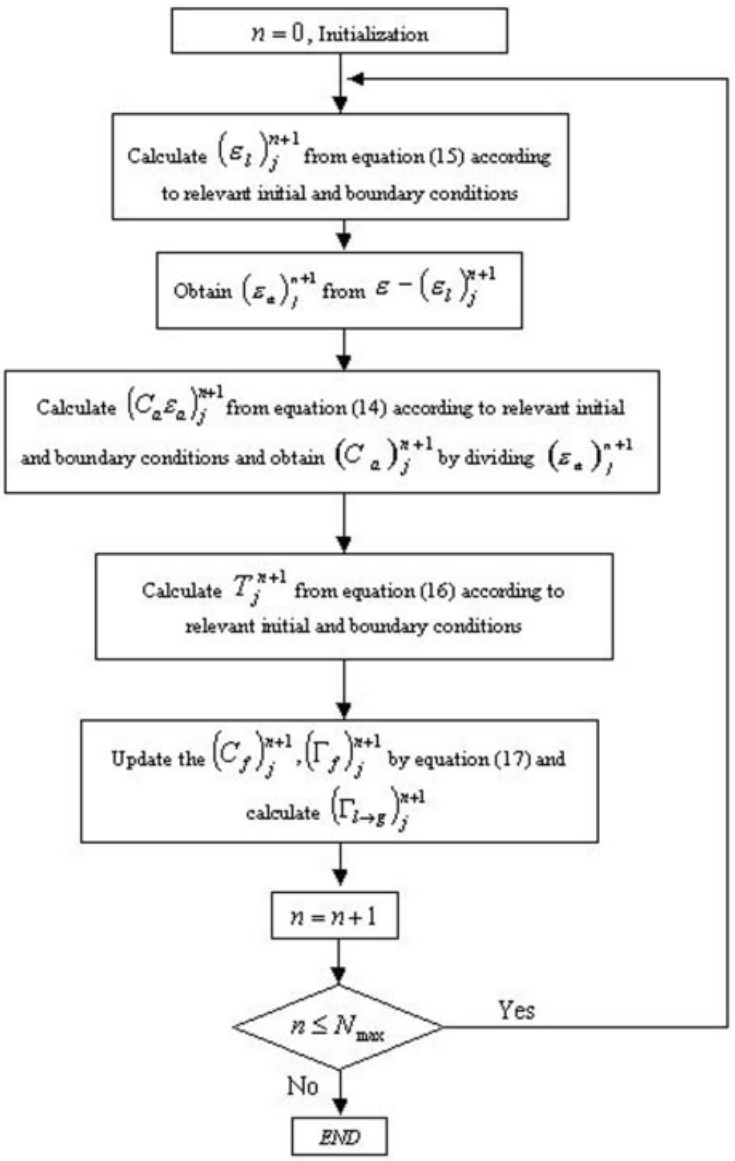

Figure 2 Flow chart of the numerical calculation.

NUMERICAL SOLUTIONS

Comparison with experimental measurements

The model is partially verified by comparing the simulation result with the experimental data published in a previous study.[11] Because of the difficulties in measuring simultaneously the dynamic change of water content in fibers, the liquid volumetric fraction distribution, and the moisture sorption rate without affecting the transport processes, we only validate the model on fabric temperature measured using noncontact infrared measurement techniques. The computational simulation was conducted on a Pentium III PC computer by developing a program written in C++.

Figure 3 shows the comparison of the computed temperature changes on the upper surface with experimental measurements for a wool slab. The temperature changes on the surface of the slab during the liquid moisture transfer process from 20.0 to 19.5°C in the initial stage, then reaches an equilibrium state. The

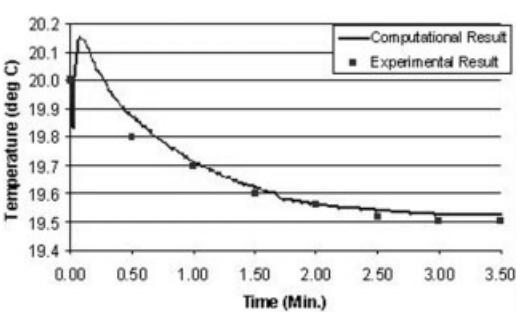

Figure 3 Comparison of computational results with experimental results.

TABLE I
Physical Properties of the Materials

Parameter	Symbol	Unit	Value
Density of the polymer fiber[18]	ρ	kg/m^3	1.31×10^3
Radius of the polymer fiber (wool)	R_f	m	1.03×10^{-5}
Porosity of polymer slab	ε		0.915
Diffusion coefficient of vapor in the fiber[4]	D_f	m^2/s	1.34×10^{-13}
Volumetric heat capacity of fiber[19]	c_{vf}	kJ m^{-3} K^{-1}	$4.184 \times 10^3 \times 1.31 \times (0.32+W_{cf}/1.0 + W_{cf})$
Thermal conductivity of slab[16]	K	$\times 10^{-3}$ W m^{-1} K^{-1}	Profiles
Heat of sorption of water vapour[19]	λ_v	kJ kg	$2522.0 + 1602.5e^{-11.72W_{cf}}$
Heat of sorption of liquid water[19]	λ_v	kJ kg	$1602.5e^{-11.72W_{cf}}$
Surface tension of liquid water[11]	γ	$\times 10^{-3}$ N m^{-1}	30
Contact angle of the polymer fiber (wool)[11]	ϕ	degree (°)	85°
Fiber emissivity[16]	ε_r		0.9
Radiative absorption constant of the fiber[3]	β	m^{-1}	74.27
Capillary radius with the maximum distribution inside the porous slab[11]	d_c	m	200×10^{-6}

computational temperature profiles are consistent with the experimental observations, indicating that the model is able to predict the temperature changes on the slab surface during the liquid diffusion process.

Computational case studies

We simulated a clothed human body with initial skin condition of (T_{sk0} = 33°C, RH_{sk0} = 50%) and being exposed to an ambient condition of (T_{env0} = 20°C, RH_{env0} = 60%). The person is assumed to move suddenly to a cold environment of (T_{env1} = 1°C, RH_{env1} = 90%) with intensive physical exercises so that the condition of skin surface is changed to (T_{sk1} = 36°C, RH_{sk1} = 99%). The contact situation at the skin–slab surface is assumed to have two cases[1]: there is no direct contact between liquid water and the slab, so that moisture transfer to the slab is by vapor diffusion (VD case)[2]; there is a direct contact between liquid water and the slab so that the liquid can diffuse into the slab by capillary action (LD case).

Values or numerical relationships for a number of the material properties and coefficients in the numerical computations are listed in Table I. The values with reference numbers were obtained from the literature and those without a reference were determined experimentally. The values of the related transfer coefficients are listed in Table II.

Figure 4 shows the dynamic temperature distributions in the porous polymer slab: (a) vapor diffusion and (b) liquid diffusion. In the case of VD, there is a temperature gradient maintained between the two surfaces of the textile slab, although the temperature close to the skin surface tends to decrease slightly after a small increase initially. On the outer surface, the temperature drops quickly from the initial 20°C to around 4°C. In the case of LD, the temperature gradient between the two surfaces is much smaller. There is a significant increase in temperature across the thickness of the slab initially, then the temperature decreases significantly throughout the slab. There are significant differences between the two cases in (1) temperature distribution across the slab and (2) the change of temperature distribution with time.

Figure 5 shows the dynamic water vapor concentration distributions in the slab for (a) the VD case and (b) the LD case. In the VD case, there is a gradient in water vapor concentration across the slab similar to the temperature distribution. In the initial stage, the vapor concentration increases significantly in the layers close to the skin surface and decreases in the outer layers. In the LD case, the gradient in vapor concentration between the two surfaces of the slab is small. The vapor concentration throughout the slab increases slightly in the initial transient period and then decreases gradually. There are significant differences between the two cases in (1) vapor concentration distribution across the slab, (2) the initial rise in vapor concentration (e.g., the maximum C_a), and (3) the change of vapor concentration distribution with time such as the minimum C_a reached in 60 min.

Figure 6 shows the dynamic distribution of the relative humidity throughout the slab for (a) the VD case and (b) the LD case. In the VD case, the relative

TABLE II
Values of Transfer Coefficients

Coefficient	n = 0	n = 1
h_{cn} (m/s)	8.8×10^{-3}	0.2×10^{-3}
h_{tn} (W m^{-2} K^{-1})	10	50
W_n (s m^{-1})	0.0	410
R_n (m^2 K W^{-1})	0	0.0054
H_{cn} (m/s)	8.8×10^{-3}	1.85×10^{-4}
H_{tn} (W m^{-2} K^{-1})	10	39.4

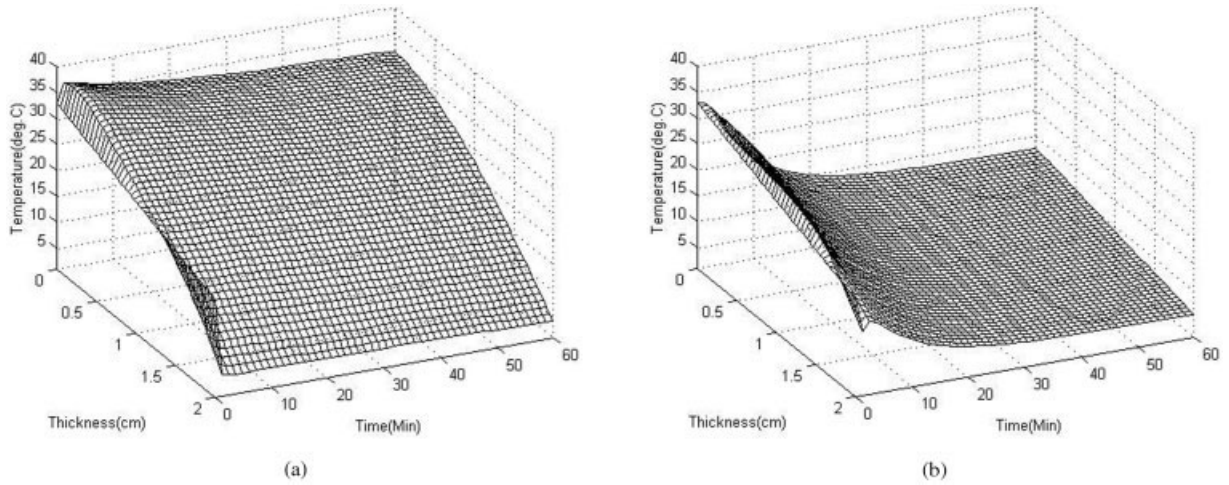

Figure 4 (a) Dynamic temperature distributions in the slab for VD case. (b) Dynamic temperature distributions in the slab for LD case.

humidity increases gradually to 100% after a rapid increase in the initial stage, especially on the two surfaces. The distribution of relative humidity is not uniform: the humidity on the two surfaces approaches saturation in a short period but those in the middle layer of the slab increase much more slowly. In the LD case, the relative humidity rises rapidly to saturation throughout the slab and becomes uniformly distributed within a few minutes.

Figure 7 illustrates the water content distribution in the fibers for (a) the VD case and (b) the LD case, which are very similar to the relative humidity distributions. In the VD case, the water content increases much faster in the fibers close to the two surfaces than it does in the middle layers of the slab. Different behavior is observed in the LD case, where the water content in the fibers reaches the level of its saturation within 10 min throughout the slab, as the relative humidity of surrounding the fibers reaches the level of 100% across the slab [Fig. 6(b)].

Figure 8 shows the dynamic distribution of the liquid volumetric fraction for (a) the VD case and (b) the LD case. In the VD case, there is no liquid water in the slab until condensation occurs on the outer surface of the slab after a 45-min exposure and the condensed liquid was transferred inwardly by the capillary force to the dry region. At the low temperature, the relative humidity can reach 100% even though the actual moisture concentration in the air is low. For instance, at 1°C the saturated water vapor concentration in the air is about 5.18×10^{-3} kg/m^3. When the water vapor concentration is greater than the saturated vapor concentration of a given temperature, the water vapor begins to condense and form liquid water. In our simulation, at the time of condensation the temperature on the outer surface of the slab is about 5.3°C,

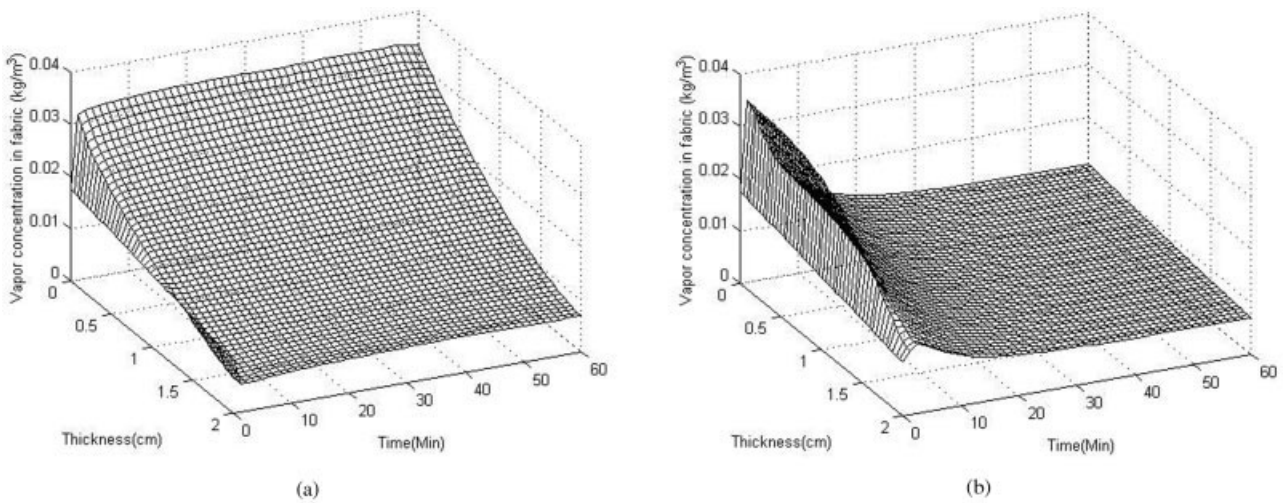

Figure 5 (a) Dynamic water vapor concentration distributions in the slab for VD case. (b) Dynamic water vapor concentration distributions in the slab for LD case.

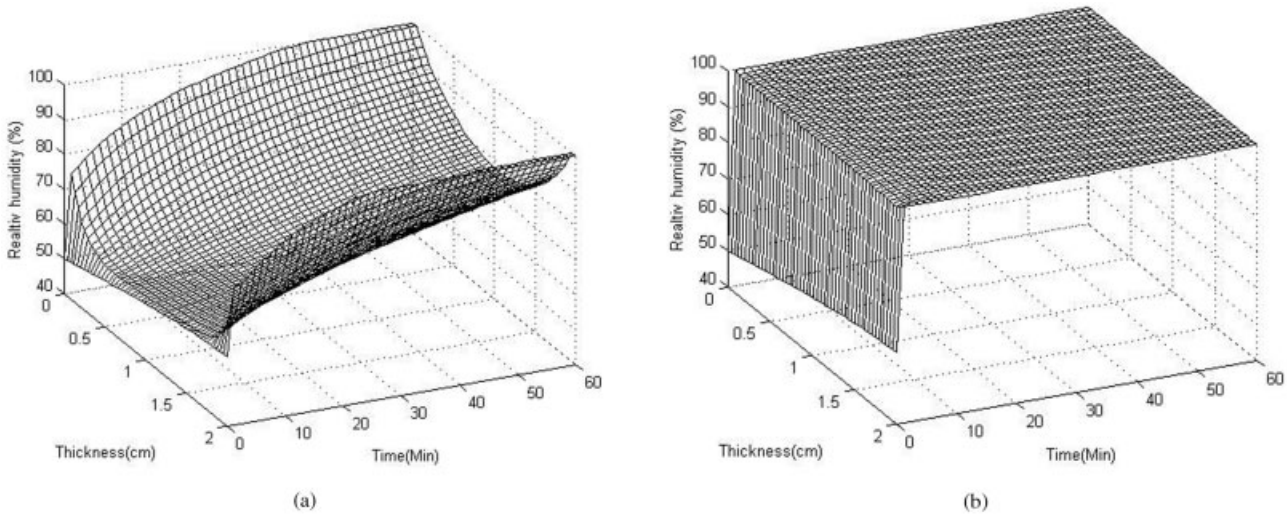

Figure 6 (a) Dynamic RH distributions in the slab for VD case. (b) Dynamic RH distributions in the slab for LD case.

with the water vapor concentration of 7.41×10^{-3} kg/m^3, which is larger than the value of the saturated concentration 6.91×10^{-3} kg/m^3. In the LD case, the capillary effect is so significant that the liquid water is transferred in a very short time, which is in the order of $t \sim L^2/D_l$, to reach the status of equilibrium. When $\varepsilon_l = \varepsilon = 0.915$, the liquid diffusivity is 3×10^{-6} m^2/s, so the shortest equilibrium time is about 133 s. This fast transfer phenomenon has a significant effect on the dynamic changes of water vapor concentration throughout the slab (Fig. 5), and consequently, the distribution of RH (Fig. 6), water content in fiber (Fig. 7), and the temperature (Fig. 4).

DISCUSSION

The computational results illustrated in these figures have outlined a complex picture of the interactions among the different ways of moisture transfer and the coupling effects between heat and moisture-transfer processes, which are discussed in detail in the following sections.

Interactions among different moisture-transport mechanisms

Vapor diffusion and liquid diffusion

The dynamic distribution of water vapor concentration is mainly determined by the gradient in moisture concentration [Fig. 5(a)] when the liquid volume in the slab is insignificant [Fig. 8(a)]. When the liquid water diffuses into the slab and dominates the void space [Fig. 8(b)], the vapor concentration distribution is mainly dependent on the temperature distribution in the slab [Fig. 5(b)]. This is attributed to the fact that

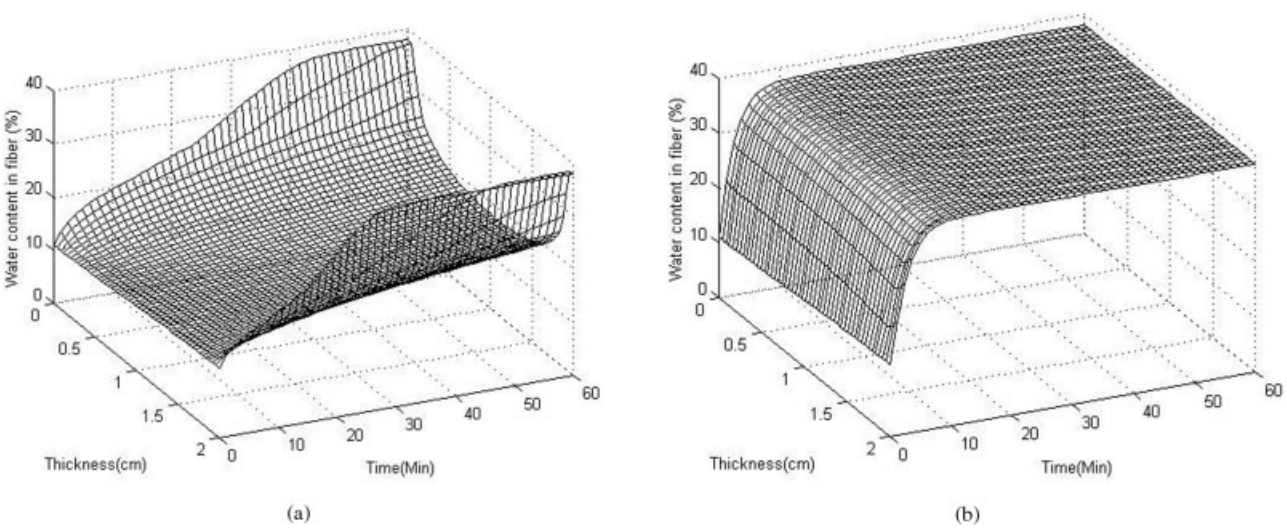

Figure 7 (a) Dynamic water content distributions in the fibers for VD case. (b) Dynamic water content distributions in the fibers for LD case.

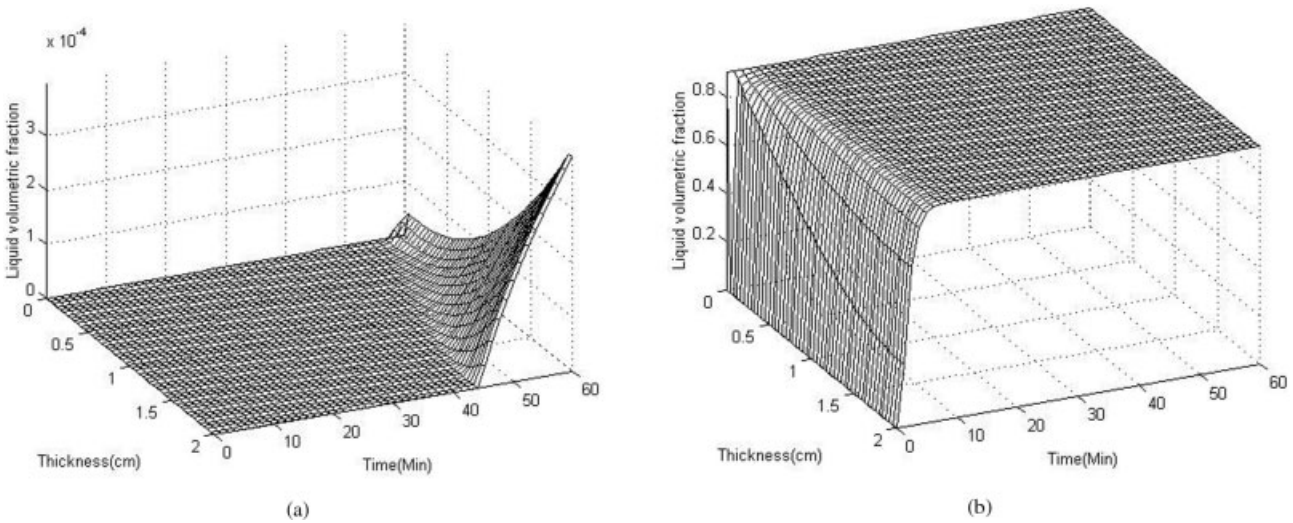

Figure 8 (a) Dynamic liquid water distributions in the slab for VD case. (b) Dynamic liquid water distributions in the slab for LD case.

moisture vapor reaches equilibrium saturation quickly with surrounding liquid water and the saturated vapor concentration is a function of the local temperature only.

Condensation/evaporation and liquid diffusion

The simulation shows the situation of moisture vapor condensation on both the inner and outer surfaces of the slab, and the mobility of condensed liquid water is dependent on the accumulation of the liquid water, the feature of the capillary pore distribution in the slab, and the interaction between liquid water and the solid surface.

When liquid water diffuses into the slab for the case of LD, fiber surfaces are covered by liquid water and the void space is filled with liquid water, so that condensation becomes negligible, except on the outer surface in the first few minutes. The evaporation rate is also negligible because there is little space for evaporation in the slab and the outer surface is sealed by a membrane with large water vapor resistance.

Coupling effects between heat transfer and moisture transfer

Heat transfer and liquid diffusion

In a comparison of Figure 4 with Figure 8, it is obvious that liquid diffusion has a very significant impact on the heat-transfer process. When liquid water diffuses into the slab and occupies the void space, the temperature gradient between the two surfaces is reduced significantly, largely attributable to the increase of overall thermal conductivity of the slab by the liquid water. This explains why we feel cold when our clothing gets wet and indicates the importance of preventing liquid water diffusion into textiles in apparel design.

Heat transfer and vapor diffusion

In a comparison of Figure 4 and Figure 5, the water vapor concentration distribution has a pattern similar to the temperature distribution in the case of LD. As liquid water diffuses into the slab and occupies most of the void space, the water vapor is assumed to reach saturation at the presence of liquid, so that the vapor concentration is the saturated concentration that is a function of temperature. When there is no or little liquid in the slab, the vapor diffusion is mainly determined by the gradient of moisture concentration except in the initial stage when fiber moisture sorption is significant.

Heat transfer and moisture sorption

The moisture content of the fibers in Figure 7(a) is highly associated with the distribution of relative humidity, which is in turn determined by the temperature and vapor concentration distributions [Fig. 6(a)]. This is because the moisture sorption rate is determined by eqs. (6) and (7), where the water concentration on the fiber surface is a function of relative humidity of the surrounding air. The fiber moisture sorption, in return, induces a significant increase of temperature in the middle to inner layers of the slab and reduces the rate of temperature drop in the outer layers of the slab [Fig. 4(a)]. In the VD simulation, the RH is forced to change from 50% at 33°C (1.77×10^{-2} kg/m^3) to 99% at 36°C (4.08×10^{-2} kg/m^3) on the skin surface. On the outer surface, the increase of RH is mainly because of the drop of the temperature from

20°C and 50% with water vapor concentration of 8.59×10^{-3} kg/m^3 to 1°C with the nearly saturated water vapor concentration of 4.67×10^{-3} kg/m^3. The RH in the middle layer of the slab is lower than that of the outer surface because the heat is released from the moisture sorption in the outer layers.

In the case of LD, the relative humidity across the slab reaches 100% rapidly, as shown in Figure 6(b), which induces a very high moisture sorption rate throughout the slab and leads to a fast increase of moisture content in the fibers [Fig. 7(b)]. Meanwhile, a rapid temperature increase across the slab is observed in the first few minutes of the liquid diffusion process attributed to the fiber moisture sorption [Fig. 5(b)]. Because the heat of liquid sorption is much lower than that of water vapor, the temperature does not increase as much as it does in the VD case. After liquid water is transferred into the slab by the capillary effect, the temperature drops quickly as discussed above.

CONCLUSIONS

In summary, a new mathematical model and a numerical solution were developed to simulate the radiation and conduction heat transfer coupled with liquid water transfer, moisture sorption, and condensation in porous polymer materials for investigating the complicated coupled interactions among them. The modeling of the complicated coupling effects among the different heat and moisture-transport processes was partially verified on the fabric temperature changes. Further computational case studies have revealed complex interactions among different modes of moisture transport and the coupling effects between heat transfer and moisture-transfer mechanisms. Significant differences were identified between different contact boundary conditions and the physical mechanisms were analyzed in detail for the situations with direct and nondirect contact of liquid water. The model can be used as an effective scientific analysis tool for the engineering design of textile materials with consideration of fiber-fabric structural features, physical properties, and chemical-physical treatments in manufacturing processes.

NOMENCLATURE

C^* Saturated water vapor concentration (kg/m^3)
C_a Water vapor concentration in the air filling the interfiber void space (kg/m^3)
C_{env} Water vapor concentration of the ambient air (kg/m^3)
C_f Water vapor concentration in the polymer fibers (kg/m^3)
C_{fs} Water vapor concentration at the fiber surface (kg/m^3)
c_v Volumetric heat capacity of the polymer porous material (kJ m^{-3} K^{-1})
D_a Diffusion coefficient of water vapor in the air (m^2/s)
D_f Diffusion coefficient of water vapor in the polymer fibers (m^2/s)
D_l Diffusion coefficient of liquid water in the polymer porous material (m^2/s)
F_L Elementary total thermal radiation incident inside the clothing traveling to the left (W/m^2)
F_R Elementary total thermal radiation incident inside the clothing traveling to the right (W/m^2)
h_{cn} Convective heat-transfer coefficient at the clothing surface ($n = 0$, inner surface; $n = 1$, outer surface) (W m^{-1} K^{-1})
H_{cn} Combined heat transfer coefficient at the clothing surface ($n = 0$, inner surface; $n = 1$, outer surface) (W m^{-1} K^{-1})
h_{lg} Mass transfer coefficient for evaporation and condensation (m/s)
h_{mn} Convective vapor transfer coefficient at the clothing surface ($n = 0$, inner surface; $n = 1$, outer surface) (m/s)
H_{mn} Combined vapor transfer coefficient at the clothing surface ($n = 0$, inner surface; $n = 1$, outer surface) (m/s)
K Thermal conductivity of the fabric (W m^{-1} K^{-1})
K_l Thermal conductivity of the liquid water (W m^{-1} K^{-1})
K_{mix} Effective thermal conductivity of the polymer porous material (W m^{-1} K^{-1})
L Thickness of the polymer porous material (m)
N_{max} Maximum time step of the calculation
r Radial coordinate of the fiber (m)
RH_{env} Relative humidity of ambient air
RH_{sk} Relative humidity of skin surface
S_v Surface volume ratio of the polymer fiber (m^{-1})
t Real time from change in calculation (s)
T Temperature of the polymer porous material (K)
T_{env} Temperature of the ambient air (K)
T_{sk} Temperature of the skin surface (K)
W_{cf} Water content of the polymer fibers
x x-coordinate for the direction of thickness (m)

Greek symbols

α Effective angle of capillaries in the polymer porous material (°)
β Radiation absorption constant of the fiber (m^{-1})
γ Surface tension (N/m)

Γ_f Effective sorption rate of the moisture (kg m^{-3} s^{-1})
Γ_{lg} Evaporation/condensation rate of the liquid/vapor (kg m^{-3} s^{-1})
ε Porosity of the polymer porous material
ε_a Volume fraction of water vapor
ε_f Volume fraction of fibers
ε_l Volume fraction of liquid phase
ε_n Thermal radiative emissivity at the clothing surface (n =0, inner surface; n = 1, outer surface)
ε_r Thermal radiative emissivity of the fiber
η Dynamic viscosity of liquid (kg m^{-3} s^{-1})
λ_l Heat of sorption or adsorption of liquid water by fibers (kJ/kg)
λ_{lg} Heat of evaporation of water (kJ/kg)
λ_v Heat of sorption or adsorption of vapor by fibers (kJ/kg)
ρ Density of the fibers (kg/m^3)
ρ_l Density of the liquid water (kg/m^3)
σ Stefan–Boltzmann constant (56.7 $\times$ 10^{-9} w m^{-2} K^{-4})
τ_a Effective tortuosity of the polymer porous material for water vapor diffusion
τ_l Effective tortuosity of the polymer porous material for liquid water diffusion
ϕ Contact angle of the liquid water on the fiber surface

The authors thank the Hong Kong Research Grant Committee for the funding of this research through the project (PolyU5111/98E) titled *Heat and Moisture Transport in Bedding Material and the Thermal Comfort of the Patient in Pediatric Wards,* and further financial support from the Hong Kong Polytechnic University.

References

1. Henry, P. S. H. Proc R Soc London 1939, 171, 215.
2. Schneider, A. M.; Hoschke, B. N. Textile Res J 1992, 32, 61.
3. Farnworth, B. Textile Res J 1983, 53, 717.
4. Watt, I. C. Textile Res J 1960, 30, 443.
5. Watt, I. C. Textile Res J 1960, 30, 644.
6. Nordon, P.; David, H. G. Textile Res J 1967, 37, 853.
7. Ogniewicz, Y.; Tien, C. L. Int J Heat Mass Transfer 1981, 24, 421.
8. Motakef, S.; El-Masri, M. A. Int J Heat Mass Transfer 1986, 29, 1503.
9. Shapiro, A. P.; Motakef, S. Int J Heat Mass Transfer 1990, 33, 163.
10. Li, Y.; Holcombe, B. V. Textile Res J 1992, 62, 211.
11. Li, Y.; Zhu, Q. Y.; Lou, Z. X. In: Numerical Simulation of Heat Transfer Coupled with Moisture Sorption and Liquid Transport in Porous Textiles, Proceedings of the 6th Asian Textile Conference, Hong Kong, 2001.
12. Gibson, P. Governing Equations for Multiphase Heat and Mass Transfer in Hygroscopic Porous Media With Applications to Clothing Materials. U.S. Army Research, Development and Engineering Center: Natick, MA, 1994.
13. Gibson, P. W.; Charmchi, M. Sen-I-Gakkaishi 1997, 53, 183.
14. Gibson, P.; Charmchi, M. J Appl Polym Sci 1997, 64, 493.
15. Li, Y.; Luo, Z. X. Textile Res J 1999, 69, 760.
16. Luo, Z. X.; Fan, J. T.; Li, Y. Int J Heat Mass Transfer 2000 43, 2989.
17. Steele, R. Textile Res J 1953, 23, 897.
18. Yao, M. Textile Material, 1st ed. China Textile Press: Beijing, 1986.
19. Rae, A.; Bruce, R. The Wool Industry Research Association Textile Data Book; Leeds, 1973.